10. 8. 2000
LHCb Muon 2000-060

Detector Physics and Performance Simulations of the MWPCs for the LHCb Muon System

Werner Riegler
CERN

Abstract

This note discusses some basic detector physics and performance parameters of the Multi Wire Proportional Chambers (MWPCs) for LHCb that were developed at PNPI [1]. Detector physics topics like chamber geometries, potentials and fields, sensitivity to imperfections, electrostatic stability, wire diameter, gas properties and signal formation are discussed. Electronics issues concerning noise, peaking time and deadtime are described as well.

Contents

Chapter 1

Introduction

A muon trigger in LHCb requires a hit in 5 muon stations within a 25 ns time window. Each station will consist of two separate double gap chambers which are Multi Wire Proportional chambers. A detection efficiency of $> 99\%$ in a 20 ns time window is required for each muon station, so each double gap chamber should have an efficiency of $> 95\,\%$. However, since the trigger requires 5 out of 5 stations the system will be much more redundant and stable to detector performance fluctuations if each double gap chamber has an efficiency of 99 % which would 'relax' the trigger requirement to 5 out of 10. Therefore one double gap chamber should have a time resolution of $< 3.5\,ns$ rms.

This note will discuss the general characteristics of the chambers as well as specifications for the front-end electronics.

Chapter 2

Electrostatics

2.1 Geometry and Fields

We assume a parallel plate geometry where the two cathode planes are at a distance of $h1 + h2$. The two cathode planes are at ground potential. In between the two planes there is an infinite row of anode wires with radius r_a at a pitch of s and distances $h1$ and $h2$ from the cathodes (Fig. 2.1).

Defining the 'equivalent cathode radius' [2] r_c by

$$\ln r_c = \ln(4\pi/h) + \ln\cos(\frac{ad}{2}) - \sum_1^\infty L_n \tag{2.1}$$

where

$$L_n = \frac{1}{2}\ln\left(\frac{\cosh ans - 1}{\cosh ans + \cos ad}\right) \tag{2.2}$$

and

$$h = (h1 + h2)/2 \qquad d = h1 - h2 \qquad a = \pi/2h \tag{2.3}$$

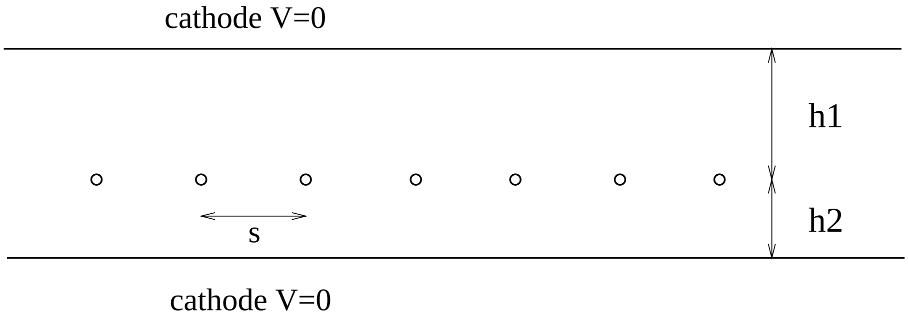

Figure 2.1 : *Wire chamber geometry.*

the capacitance per unit of wire length can be expressed as

$$C = \frac{2\pi\epsilon_0}{\ln\frac{r_c}{r_a}} \tag{2.4}$$

and the field close to the anode wires is given by

$$E(r) = \frac{V_a}{r\ln\frac{r_c}{r_a}} \tag{2.5}$$

For the symmetric case ($h1 = h2 = h, d = 0$) we have

$$L_n = \ln\tanh\frac{n\pi s}{4h} \tag{2.6}$$

and if $\cosh\frac{2\pi h}{s} >> 1$, the above formulas can be approximated and the field on the wire surface (E_a) and the cathode surface (E_c) for a given anode wire voltage are given by

$$r_c = \frac{s}{2\pi}e^{\frac{\pi h}{s}} \qquad E_a = \frac{V_a}{r_a\ln(\frac{r_c}{r_a})} \qquad E_c = \frac{V_a\pi}{s\ln(\frac{r_c}{r_a})} \tag{2.7}$$

Figures 2.2 and 2.3 show the values of the above numbers for a set of chamber parameters.

2.2 Imperfections

A number that is very important for the chamber construction is the sensitivity of the wire surface field to chamber imperfections. The imperfections will result in gas gain variations which should however not exceed ±20% across an entire chamber. We will see later that a gas gain change of 20% corresponds to a wire surface field change of about 1%. To see how this requirement translates into specifications on wire positions and cathode flatness we consider four different scenarios (the wire pitch is 1.5 mm). The calculations were done with GARFIELD [3].

- Figure 2.4 shows the field change for a Y-offset of *all* the wires (see Fig. 2.1). We find a maximum allowed offset of 300 μm for the 5 mm gap and 200 μm for the 3 mm gap.

- Figure 2.4 shows the field change for different gap sizes. This figure specifies the local cathode flatness. We find 75 μm for the 5 mm gap and 55 μm for the 3 mm gap. The gap variation i.e. the local flatness puts the most stringent specification.

- Figure 2.5 shows the sensitivity to a Y-offset of a *single* wire while keeping everything else in perfect position. An offset of 250(200) μm is acceptable.

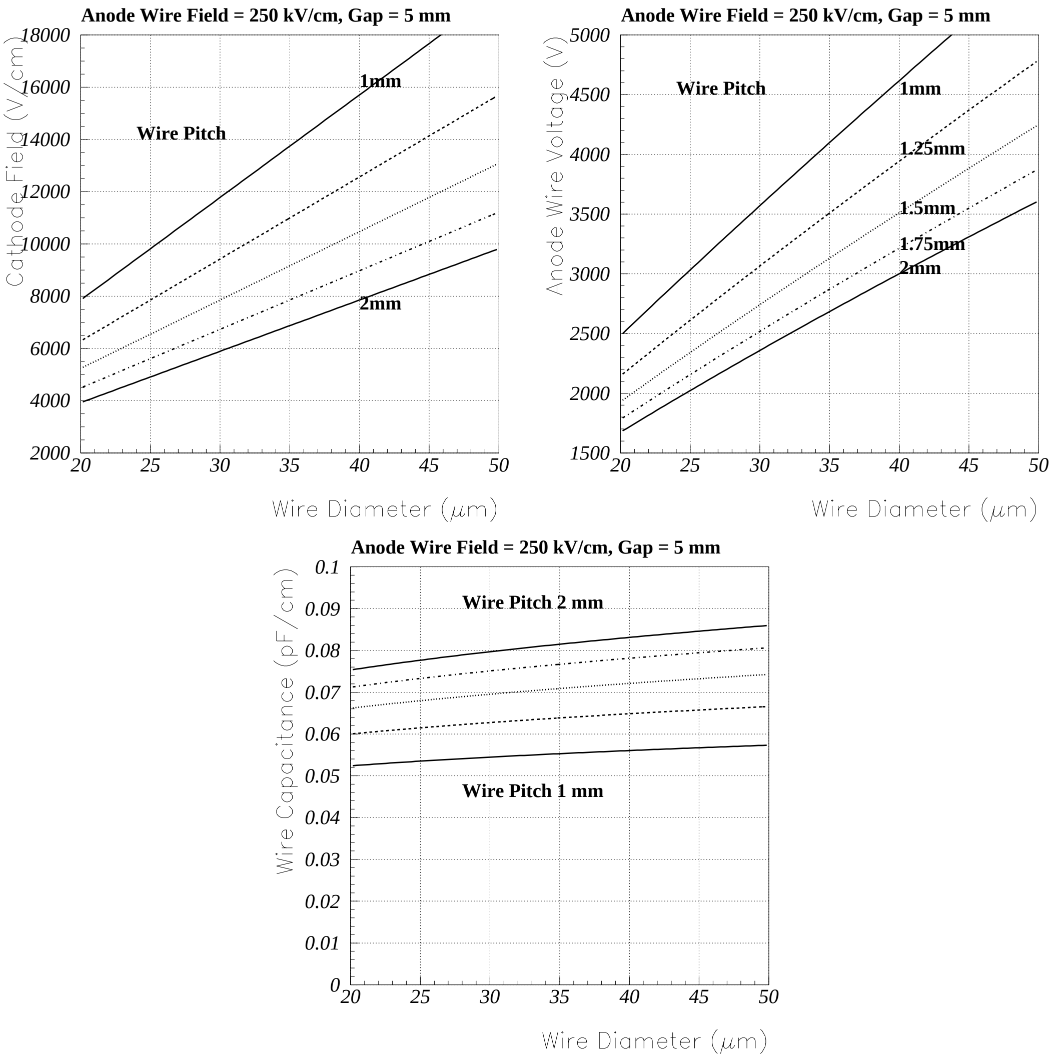

Figure 2.2 *: The top left plot shows the cathode surface field for an anode wire surface field of 250 kV/cm. The right plot shows the required anode wire voltage. The bottom plot shows the capacitance/length for a single wire.*

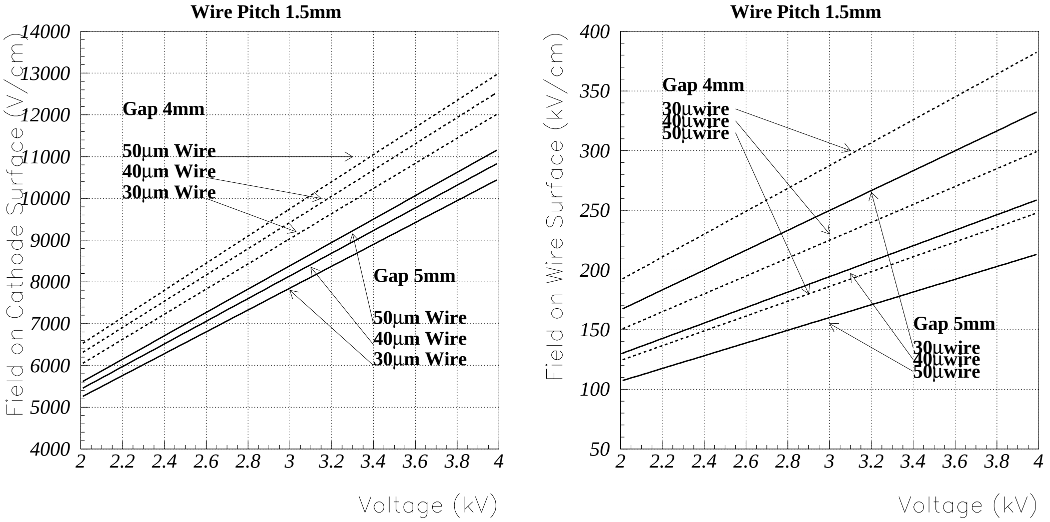

Figure 2.3 *: The left plot shows the cathode surface field for a given wire voltage. The right plot shows the corresponding wire surface fields.*

- Figure 2.5 shows the sensitivity to an X-offset of a single wire. An offset of 90-100 μm is acceptable with a very weak dependence on the gap.

The above calculations were done for a 30 μm wire, but they are not very much different for a 50 μm wire.

2.3 Guard Wires

If we just stop the wires at the end of the chamber, the fields on these last wires would be very high which we have to avoid. Assuming a 30 μm wire, 1.5 mm pitch, a gap of 5 mm and a voltage of 3.15 kV the fields on the wire surface starting from the edge wire would be 325, 277, 266, 263, 262, 262 ... kV/cm, so only the fourth wire from the edge has the nominal field, all the others have much higher fields and therefore higher gas gain.

In order to avoid this problem we put a 100 μm guard wire at the same pitch of 1.5 mm. The field is then 126 kV/cm on the guard wire and 262 kV/cm already on the next neighbour. The gas gain on the 100 μm wire is estimated to 3×10^4 assuming the extrapolation given below.

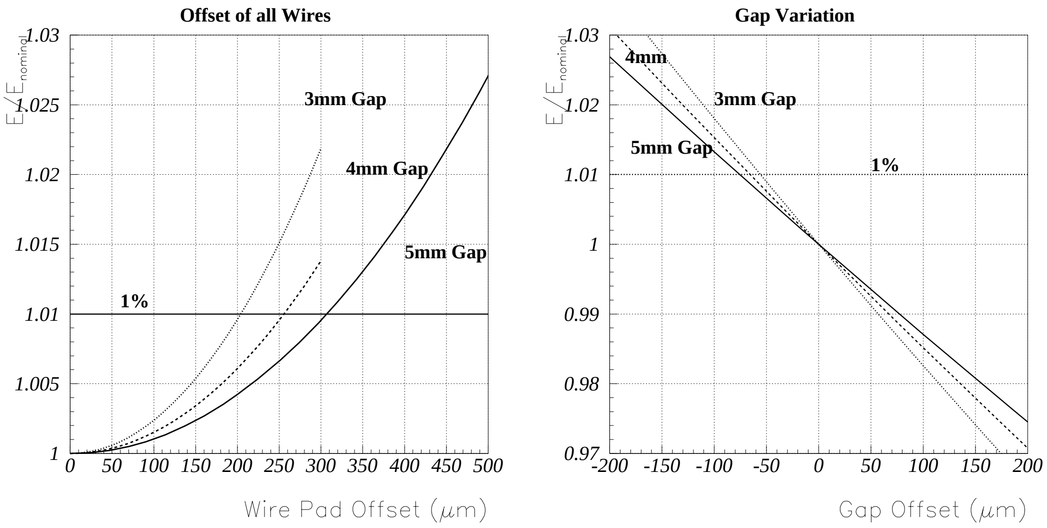

Figure 2.4 *: The left figure shows the field change for a vertical offset of all the wires. The right figure shows the sensitivity to the gap size. A gap offset of 100 μm for a 5 mm gap corresponds to a total gap of 5.1 mm with the wires in the center. Increasing the gap decreases the field.*

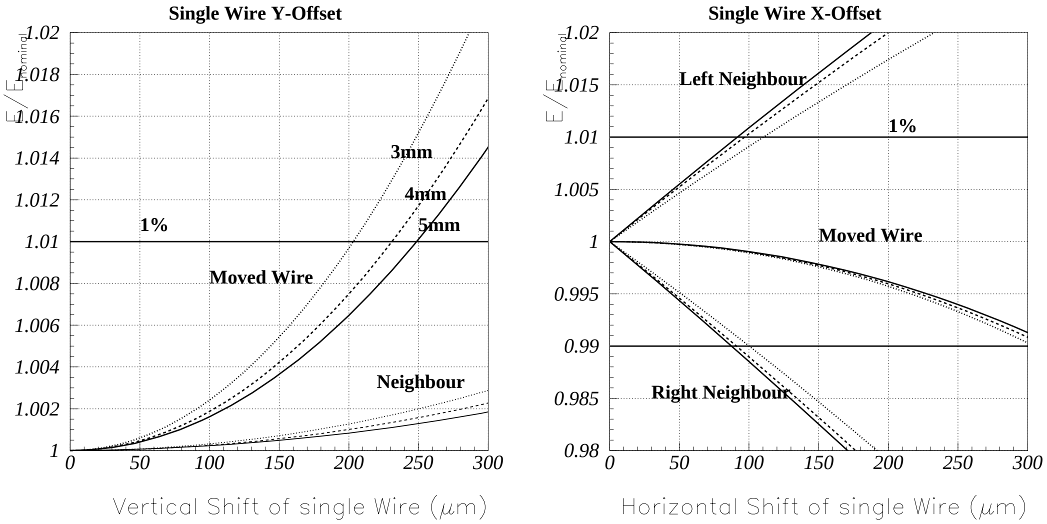

Figure 2.5 *: Moving the wire vertically increases the field on the wire and the neighbours. Moving the wire to the side increase the field on the far neighbour and decreases the field on the close neighbour. The fields are averaged around the wire.*

2.4 Stability

In addition to the gravitational force the wires are subject to electrostatic forces due to the anode wire voltage. The wires exhibit electrostatic repulsion while the cathode attracts the wires. Therefore there is a maximum allowed voltage in order to avoid instabilities. Two kinds of instabilities can occur in our chambers. First, the gravitational sag is amplified by the voltage since the wires are attraced to the 'bottom' cathode. At some point the anode wires will touch the cathode which of course should be avoided. Second the wires experience electrostatic repulsion such that for a certain voltage the stationary state prefers the wires to be in a ZigZag order. Whatever limit occurs first sets the maximum allowed voltage in the chamber. In our case the second instability sets the limit. The voltage maximum for the ZigZag instability is given by [4]

$$V < \frac{s}{lC}\sqrt{4\pi\epsilon_0 T} \quad \text{or} \quad l < \frac{s}{r_a E_{surf}}\sqrt{\frac{T}{\pi\epsilon_0}} \tag{2.8}$$

where s is the wire pitch, l the wire length, C the capacitance per unit of length, T the wire tension and E_{surf} is the electric field on the wire surface. For our (symmetric) chamber this approximately evaluates to

$$V \leq 59\sqrt{T}\left(\frac{h}{l} + \frac{s}{\pi l}\ln(\frac{s}{\pi d})\right) \tag{2.9}$$

where d is the wire diameter, T the tension in gramme and V the voltage in kV.

Before applying this criterion to our geometry we have to know the voltage range that we intend to use. The operating point will be discussed later. We infer the gas gain vs. voltage curves for different wire diameters from a measurement done with a $30\,\mu m$ wire [5] and extrapolating with Diethorn's formula [12] which parametrizes the gain with two parameters E_{min} und ΔV.

$$G = \left(\frac{V}{r_a \ln\frac{r_c}{r_a} E_{min}\frac{\rho}{\rho_0}}\right)^{\frac{V\ln 2}{\ln\frac{r_c}{r_a}\Delta V}} = \left(\frac{E_{surf}}{E_{min}\frac{\rho}{\rho_0}}\right)^{\frac{r_a E_{surf}\ln 2}{\Delta V}} \tag{2.10}$$

The fit to the gain curve for the Gas Ar/CO_2/CF_4 40/50/10 for the $30\,\mu m$ wire gives

$$E_{min} = 46.501\,kV/cm \qquad \Delta V = 42.027\,V$$

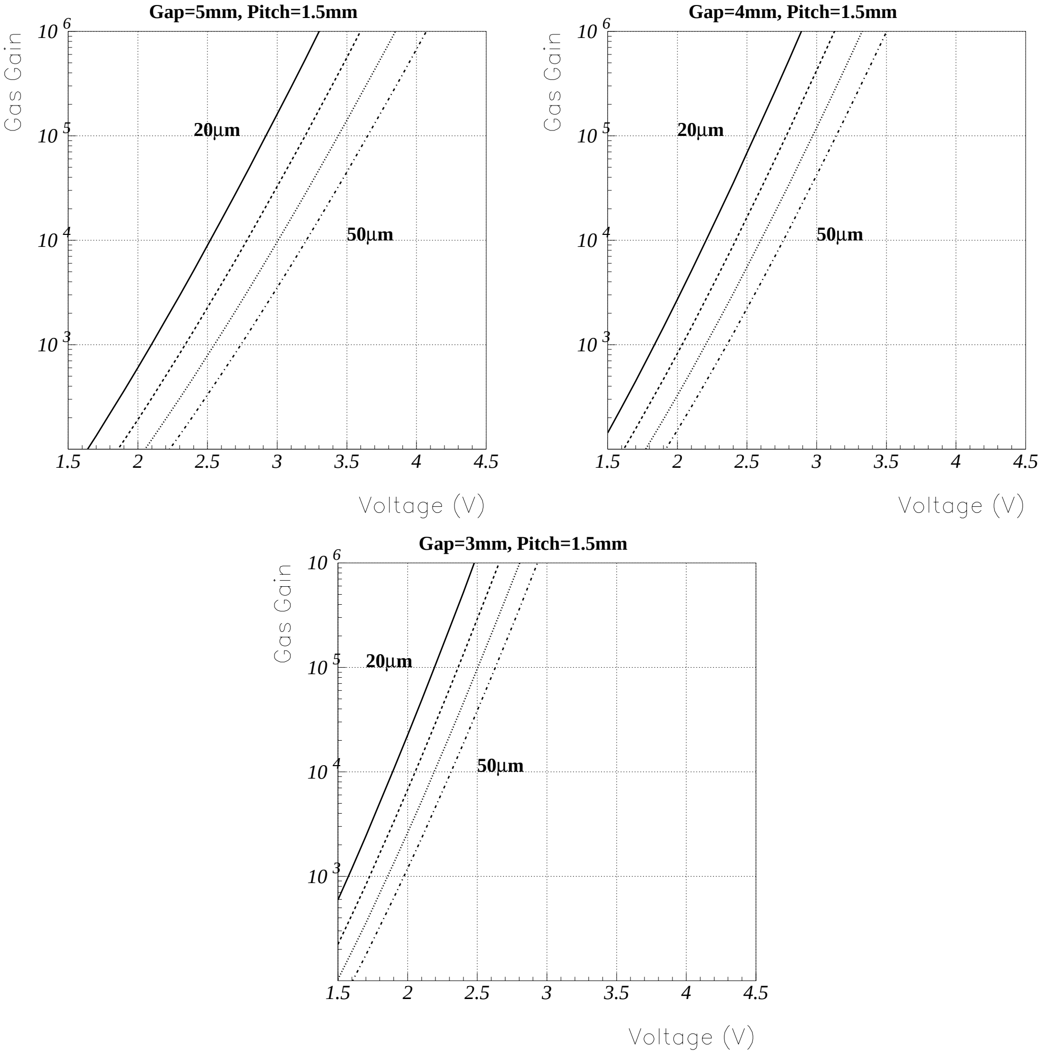

Figure 2.6 *: Gas gain versus voltage for different gap sizes and wire diameters.*

Fig. 2.6 shows the gas gain versus voltage for different gaps and wire diameters. The operating point is at a gain gain of 10^5, a gas gain $> 10^6$ is very unlikely to be used, so we set it as a maximum. Fig. 2.7 shows the voltage for a gain gain of 10^5 and 10^6 for different gap sizes.

Using the above formula (2.9) together with the maximum voltages we find the maximum allowed wire length

$$l \leq \frac{59\sqrt{T}}{V_{max}} \left(h + \frac{s}{\pi} \ln(\frac{s}{\pi d}) \right) \tag{2.11}$$

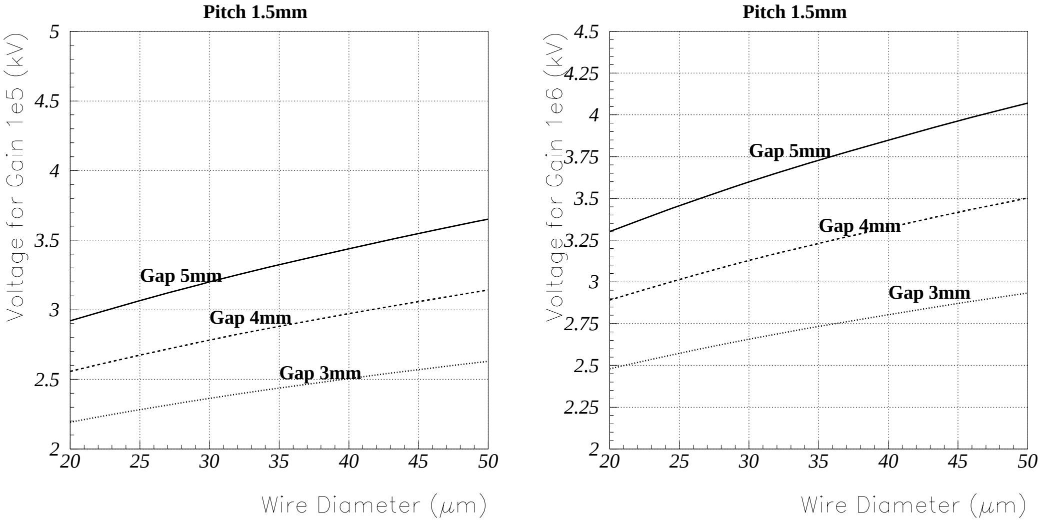

Figure 2.7 *: Required voltages for a gas gain of* 10^5 *and* 10^6*. The curve for a 30* μm *wire is from a measurement. The curves for the other wire diameters are predicted with Formula 2.10.*

Fig. 2.8 shows the maximum allowed wire lengths for different wire diameters and gaps. The fact that the limit is independent of the gap size is evident from Equation 2.8 which says the for a given wire diameter and surface field (=gas gain) the maximum allowed wire length is proportional to the wire pitch but independent of the gap size. To get the values for other tensions one has to scale with $\sqrt{T}$. Because of unavoidable imperfections of the chamber the actual wire length should be well below this limit.

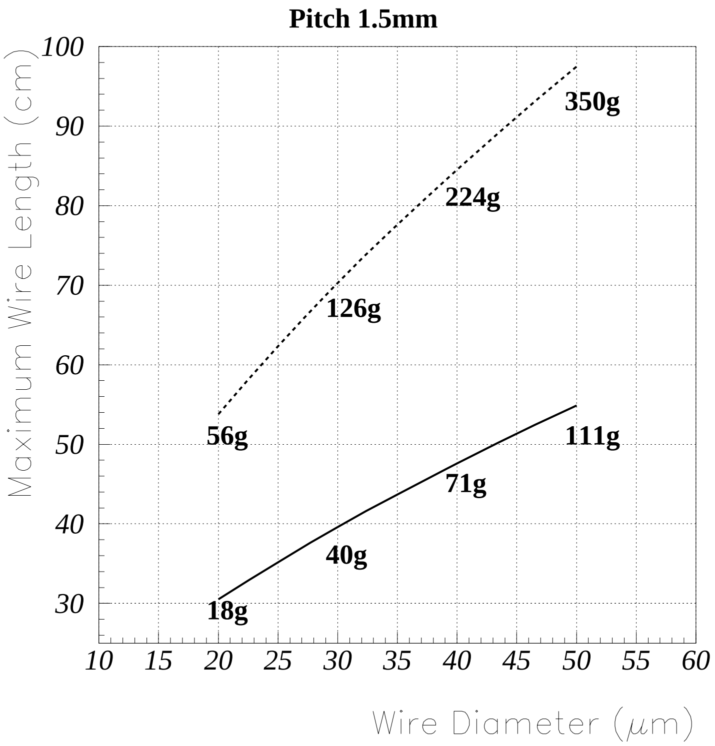

Figure 2.8 : *Maximum wire lengths for different wire diameters. For a given gas gain, the limit is independent of the gap size. The limit scales with the wire pitch i.e. for a wire pitch of 1 mm the numbers are a factor 1/1.5 lower.*

Chapter 3

Gas Properties

In this chapter we want to explore the properties of several gas mixtures that are under discussion. The baseline components are Ar, CO_2 and CF_4.

3.1 Charge Deposit

A charged particle traversing the chamber will ionize the gas along it's track. The number of interactions per unit of length is Poisson distributed since the interactions are independent. In an interaction the gas atom gets either excited or ionized. The ionization electron can have enough energy to ionize further gas atoms very close to the primary interaction. Due to these mechanisms the charged particle leaves localised clusters of electrons along it's track. The calculations were done with HEED [7]. Fig. 3.1 shows the number of interactions along a track length of 5 mm. The energy dependence follows the characteristic Bethe-Bloch form.

The probability to liberate a certain number of electrons per interaction is given in Fig. 3.2. The probability of about 3% for a cluster size of 0 electrons accounts for the interactions where the gas atom is only excited.
The minimum energy a muon must have in order to traverse all 5 muon stations is 6 GeV, which is already close to the plateu of the dE/dx curve. The 'average' number of electrons per cluster is ill-defined since the cluster size distribution has very long tails. Assuming an average number of 2.2 to 2.4 electrons is reasonable.

3.2 Drift Velocity

The MAGBOLTZ simulations of the drift velocity versus electric field for several gas mixtures is shown in Fig. 3.3. For low fields the CO_2 slows the gas down. For high fields

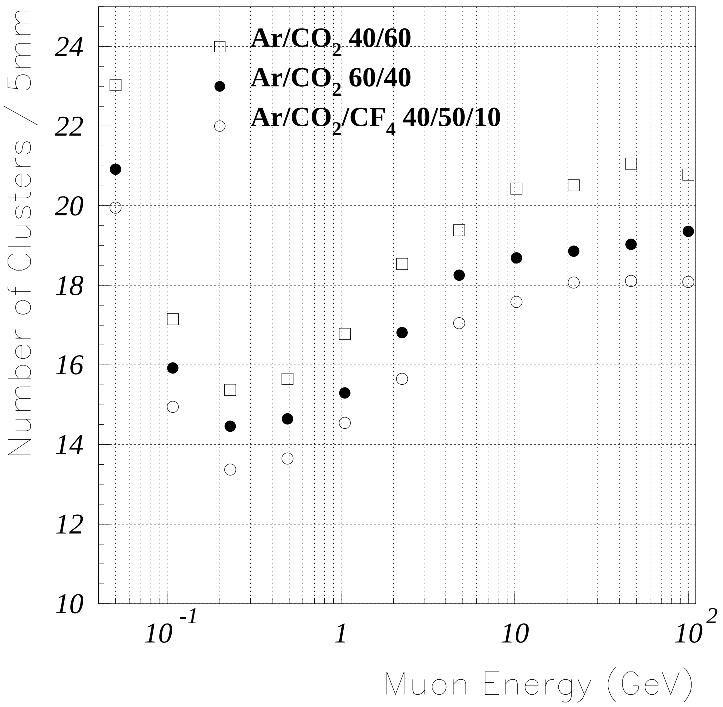

Figure 3.1 : *Energy dependence of the average number of interactions for a track length of 5 mm. The actual numbers are Poisson distributed around these mean values.*

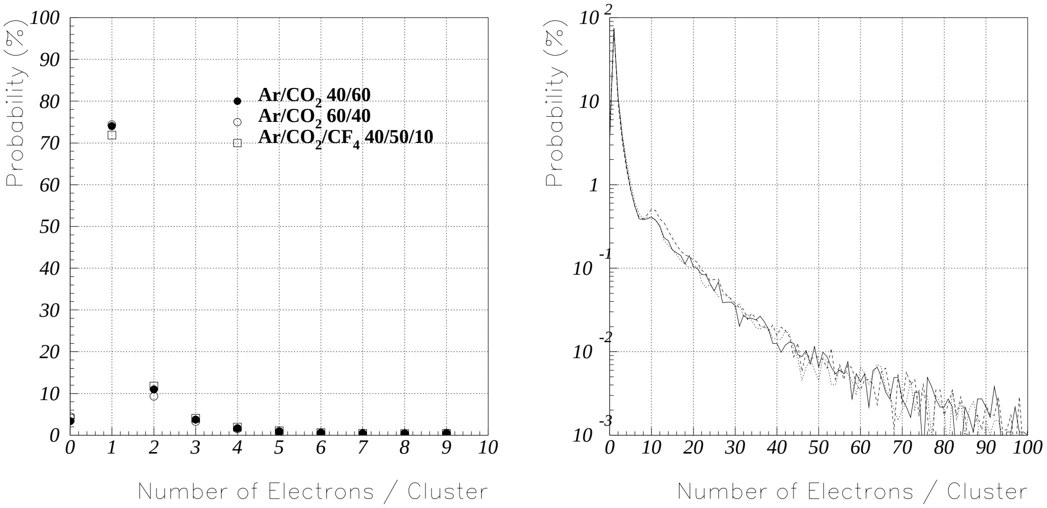

Figure 3.2 : *Cluster size distribution for three different gases for a muon energy of 6 GeV. The finite probability for a cluster size of 0 accounts for interactions where a gas atom is just excited. The right figure shows the same plot on a log scale to show the probabilities for large clusters.*

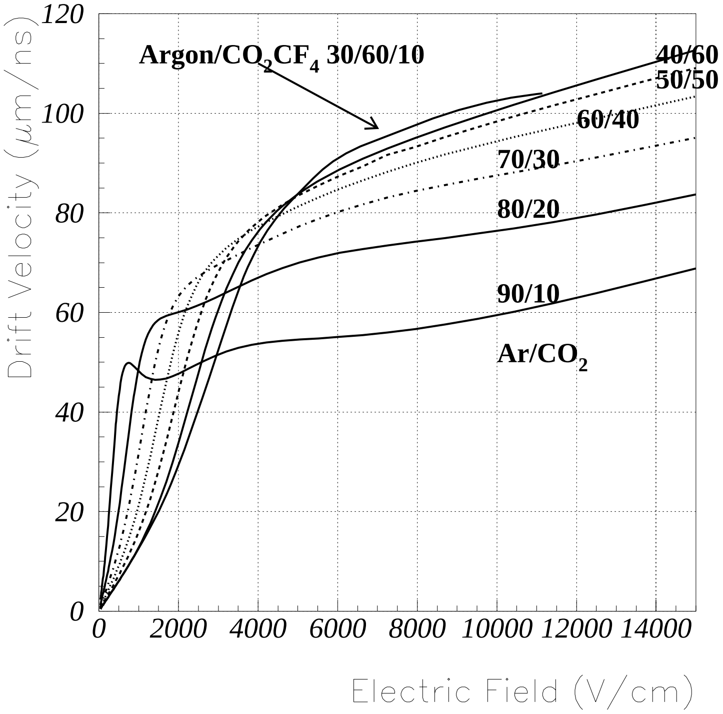

Figure 3.3 *: Drift velocity versus electric field for several gas mixtures as calculated by MAGBOLTZ. The fields in the WPC/CPC chambers are between 8000 and 10000 V/cm.*

i.e. in our case the CO_2 speeds the gas up. The CF_4 does not change the drift-velocity for large CO_2 contents. It is only used to improve the aging properties. For our MWPC fields (8-10 kV/cm) the drift-velocity is between 90 and 100 μm/ns.

The electric field across a chamber is shown in Fig. 3.4. The average arrival time of the first electrons from tracks at different distances from the wire can be seen in Fig. 3.5.

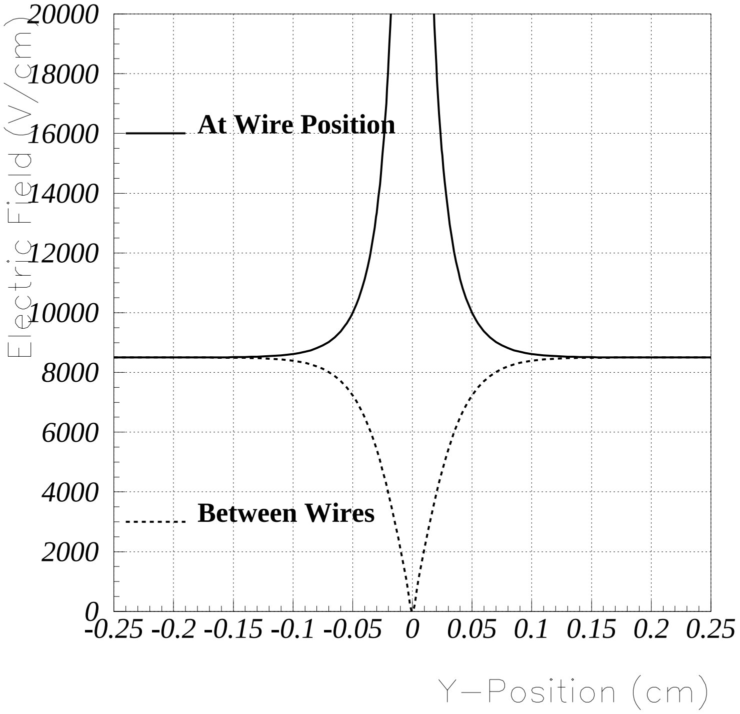

***Figure 3.4** : Electric field across a chamber with wire diameter 30 μm, pitch=1.25 mm, gap=5 mm, V_a=3000 V.*

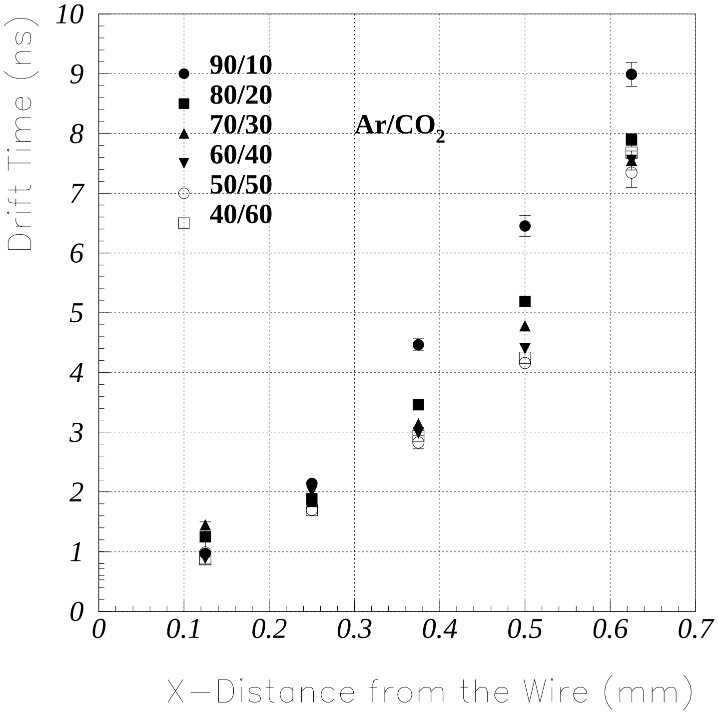

Figure 3.5 *: Arrival time of the first electrons for different distances from the wire. The chamber parameters are the same as in Fig. 3.4.*

Chapter 4

Signals

An electron moving to the anode wire will start an avalanche at about one wire radius above the wire surface. Typical amplifications in our chamber are $5 \times 10^4 - 2 \times 10^5$. The movement of the electrons and the ions created in the avalanche induces a current signal on all the electrodes in the chamber.
A single ion is moving close to the wire surface (assuming a constant ion mobility i.e. $v = \mu E$) according to

$$r(t) = r_a \sqrt{1 + \frac{t}{t_0}} \qquad \text{with} \qquad t_0 = \frac{r_a^2 \ln \frac{r_c}{r_a}}{2 V_a \mu} \tag{4.1}$$

so at time t the ion experiences a field of

$$E(t) = \frac{V_a}{\ln \frac{r_c}{r_a} r_a} \frac{1}{\sqrt{1 + \frac{t}{t_0}}} = \frac{E_a}{\sqrt{1 + \frac{t}{t_0}}} \tag{4.2}$$

This movement induces a current [12] of

$$i(t) = -\frac{q}{V} v(t) E(r(t)) = \frac{q}{2 \ln \frac{r_c}{r_a}} \frac{1}{t + t_0} \tag{4.3}$$

The current signal induced on the electrodes by the avalanche electrons moving towards the wire and the ions moving away from the wire has however a very complex form for short times: the electrons move towards the wire at very high speed and are collected within a time of less than 50 ps, therefore inducing a δ-pulse current. The speed of the ions is about three orders of magnitude smaller than that of the electrons and is given by $v = \mu \times E$ where μ is the ion mobility which is constant at low fields. At high fields however the ion mobility is not constant but $\propto 1/\sqrt{E}$. For Ar^+ ions in Ar this happens for fields $> 75\,\mathrm{kV/cm}$. For a voltage of 3.2 kV i.e. a wire surface field of 315 kV the ion is reaching a distance with a field $< 75\,\mathrm{kV}$ only after $16 t_0$ ns. In addition, the ions do not start from the wire surface but from their point of creation. Therefore close to the wire the ion current has NOT the 'traditional' $1/(t + t_0)$ form.

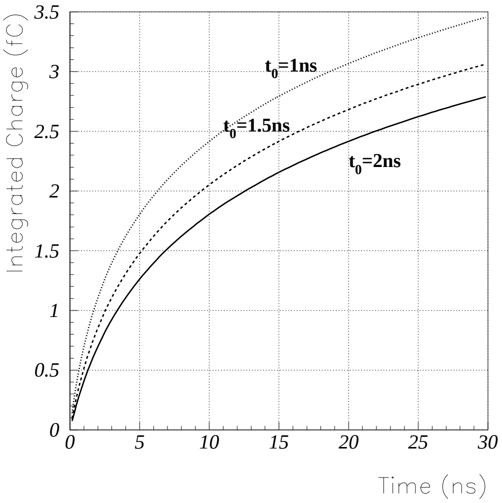

Figure 4.1 *: Integrated charge for a single primary electron and a gas gain of* 10^5.

However since the electron pulse is much shorter than the preamp integration time (peaking time) and since the non-constant ion mobility is affecting the signal shape also only at times comparable to the integration time we can still model the total induced current signal as

$$i(t) = \frac{q}{2\ln\frac{r_c}{r_a}}\frac{1}{t+t_0} \tag{4.4}$$

which gives a reasonable approximation for purposes of front-end optimization. We should however keep in mind that this is only an effective model and that the actual induced current has a much more complex form. Therefore the simulated pulse-height (induced charge in the first nanoseconds) is affected by a large error.

Using the above model, the total charge induced after a time t is then

$$Q(t) = \frac{q}{2\ln\frac{r_c}{r_a}}\ln(1+\frac{t}{t_0}) \tag{4.5}$$

Fig. 4.1 shows the induced charge versus time for a single primary electron in the chamber and a gas gain of 10^5. This figure together with the fact that we expect on average 100 primary electrons in the chamber sets the scale for the required front-end sensitivity.

For the following discussion we assume a front end electronics delta response of

$$f(t) = n^{-n}e^{n}\left(\frac{nt}{t_p}\right)^{n}e^{-\frac{nt}{t_p}} \tag{4.6}$$

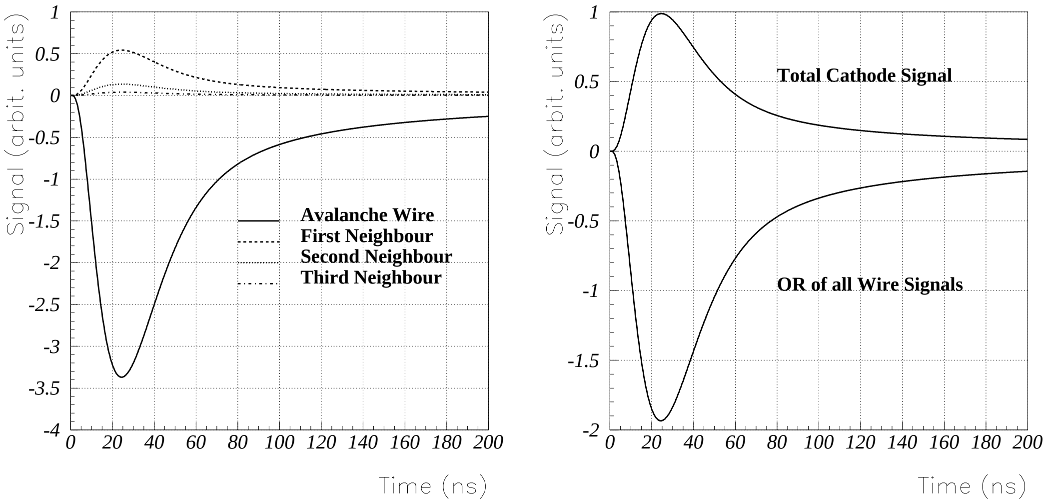

Figure 4.2 *: The left plot shows the signals induced on the individual wires. The right plot shows the 'OR' of all the wire signals and the signal induced on the cathode plane. Since the sum of all the induced signals in the chamber must add up to zero, each cathode signal has half the size of the anode signal.*

where t_p is the amplifier peaking time which we assume to be 15 ns. n is the number of integration stages which we assume to be 2. The electronics output signal is given by the convolution of the induced current signal and the delta response.

$$out(t) = \int_0^t f(t-t')i(t')dt' \tag{4.7}$$

Fig. 4.2 shows the signals induced on different electrodes. The signal on the wire where the avalanche happens is negative. The cross induced signals on the other wires and the cathode planes are positive. The required position resolution for LHCb ranges from 1 cm up to 8 cm, so we connect several wires to one preamplifier. Therefore the 'OR' of the wire signals has reduced amplitude.

Since the sum of the induced signals on all the electrodes is zero, the cathode signals (in a symmetric chamber) have half the size of the anode signal. We call the 'ORed' wires a WIRE PAD.

The signal induced on the cathode has a distribution which is given in Fig. 4.3. It shows an exact calculation done with GARFIELD. In order to achieve the required position resolution using the cathode signals, the cathode is segmented into CATHODE PADS.

If the avalanche happens on a wire which is exactly in between two cathode pads, each pad sees exactly half the total cathode signal (i.e. a quarter of the anode signal). If the avalanche happens on a wire with a distance X from the cathode pad edge, the ratio of the induced signals is given in Fig. 4.3. E.g. for a 5 mm gap a ratio of 100/1 is given for a distance of 7.5 mm.

Next we want to consider the induced current signals for a wire pad for a double gap chamber. For the calculation we use HEED, MAGBOLTZ and GARFIELD. The chamber parameters are: gap 5 mm, pitch 1.5 mm, wire 30 μm, gain 10^5. We use two gaps with staggered wires, i.e. the second gap is shifted by half the wire pitch. The tracks are randomly distributed and always perpendicular to the wire plane. Fig. 4.4 shows 4 typical current signals.

Figure 4.5 shows the arrival time distribution of the first electron. This corresponds to the intrinsic chamber resolution which is around 1 ns. The same Figure also shows the arrival time of the last electron which has an average of 25 ns.

To get a feeling for the total induced charge Fig. 4.6 shows the total induced charge in the first 5,10,15,20 ns after the arrival of the first electron.

Before studying the time resolution including the electronics we discuss the electronics parameters.

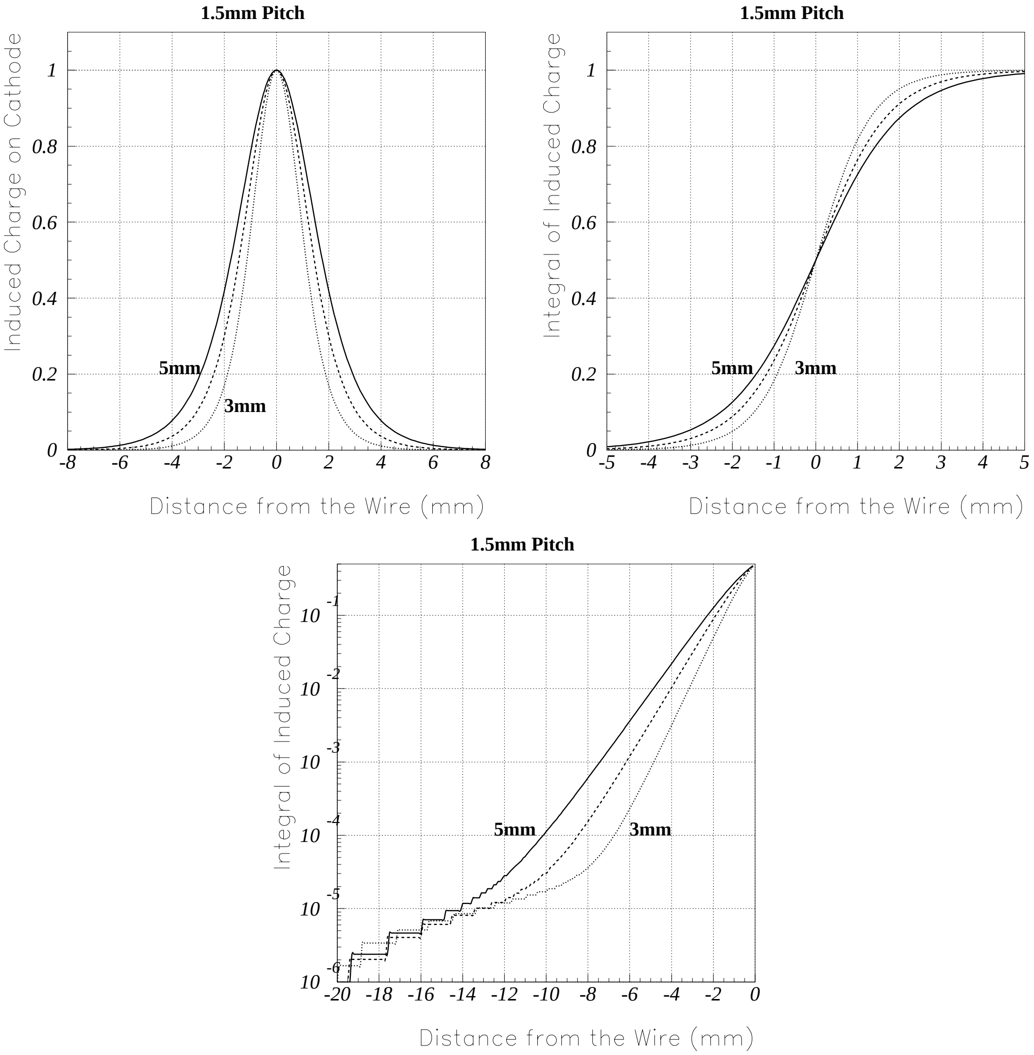

Figure 4.3 *: The first figure shows the charge distribution on the cathode. The second figure shows the integral. The third figure shows the integral on a log scale. If e.g. the avalanche happens on a wire at a distance of 7.5 mm from the cathode pad border (for a 5 mm gap), 99% of the charge is induced on the one pad and 1% is induced on the neighbouring pad.*

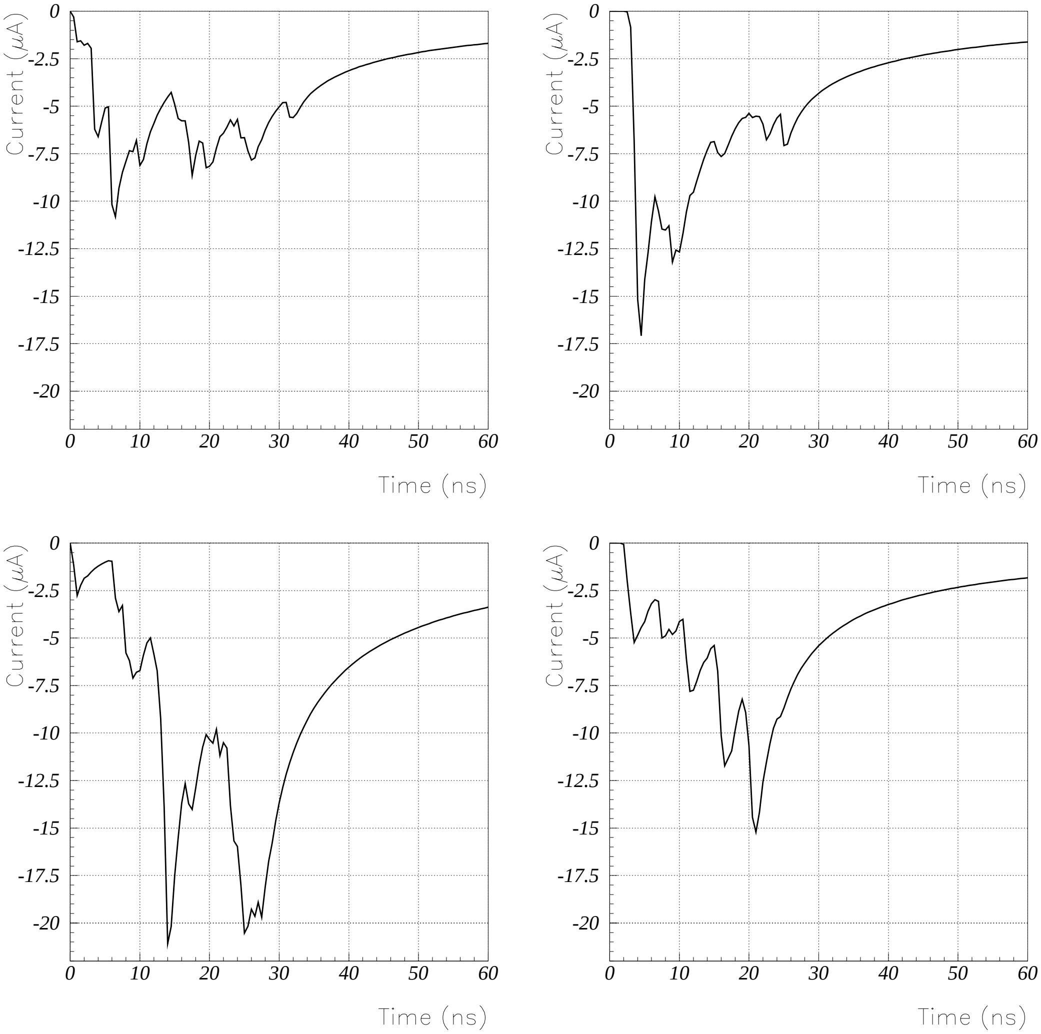

Figure 4.4 : *Typical signals induced on a wire pad. The 'spikes' show the arrival of the individual electrons.*

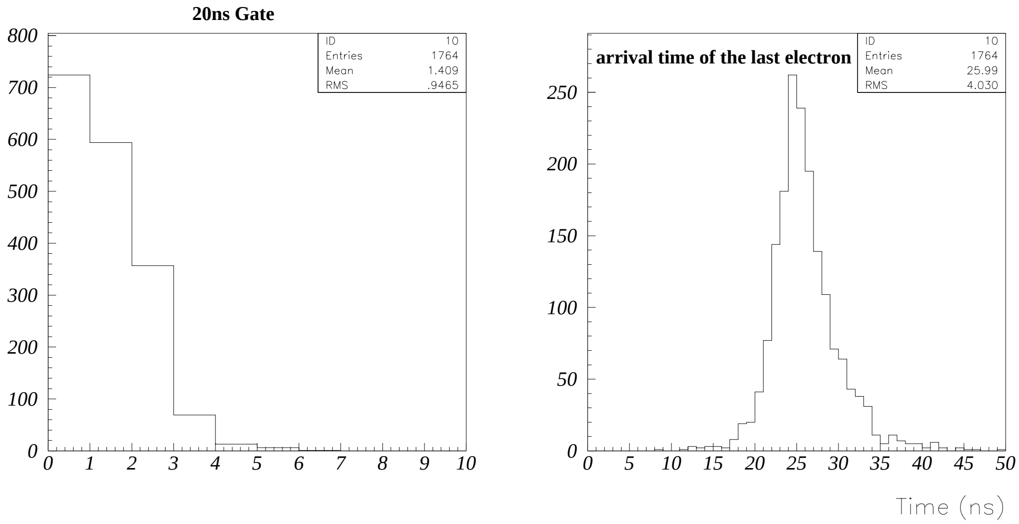

Figure 4.5 : *The left figure shows the arrival time of the first electron in a double gap chamber with staggered wires. It gives the intrinsic chamber resolution. The right figure shows the arrival time of the last electron which, together with the signal tail, determines the chamber deadtime.*

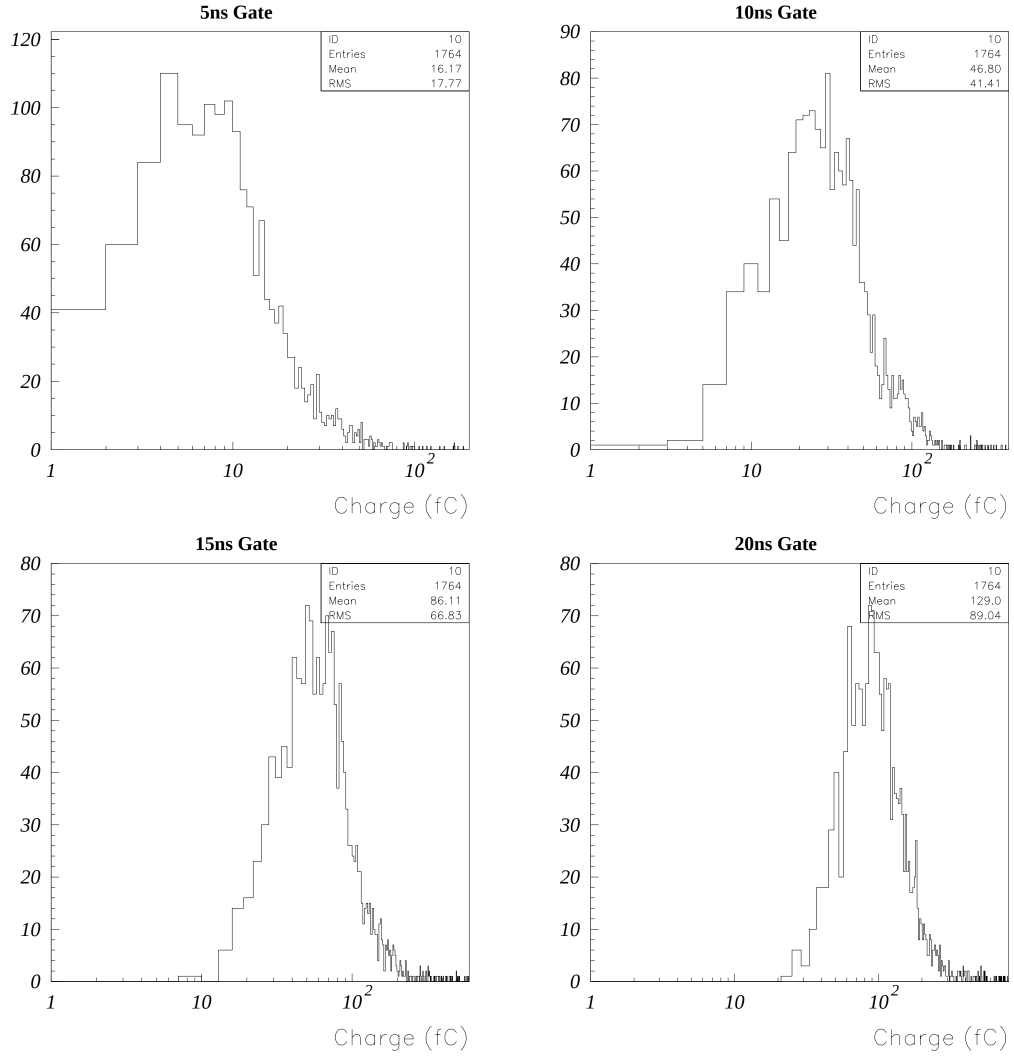

Figure 4.6 *: Total induced charge on a wire pad for different times after the arrival of the first electron.*

Chapter 5

Electronics

In order to achieve good timing resolution at reasonably low gas gain, the front-end electronics is required to have short peaking time (around 10 ns) and low noise for detector capacitances of up to 200 pF. The high rates in some of the detector regions require in addition optimized tail cancellation and baseline restoration circuits as well as radiation hard technologies.

5.1 Noise Characteristics

We characterize the front-end electronics by it's delta response $f(t)$, i.e. the front end output signal for a delta function input. For our discussion we assume, as before, a delta response of the form

$$f(t) = n^{-n} e^{n} (\frac{tn}{t_p})^{n} e^{-\frac{tn}{tp}} \tag{5.1}$$

where t_p is the peaking time and n corresponds to the number of integration stages. The output $g(t)$ of the front-end for a general current input $i(t)$ can the be computed by convoluting with the delta response

$$g(t) = \int_0^t f(t-t')i(t')dt' \tag{5.2}$$

The equivalent noise charge due to serial and parallel noise is given by [9]

$$ENC^2 = \frac{1}{2} e_n^2 C^2 \int_{-\infty}^{\infty} f'(t)^2 dt + \frac{1}{2} i_n^2 \int_{-\infty}^{\infty} f(t)^2 dt \tag{5.3}$$

where $f(t)$ is the front-end electronics delta response normalized to give and output voltage peak of unity for an input current delta function of charge unity. C is the total capacitance at the front-end input (detector capacitance+ trace capacitance + amplifier input capacitance). e_n and i_n are the spectral series and parallel noise densities. These values

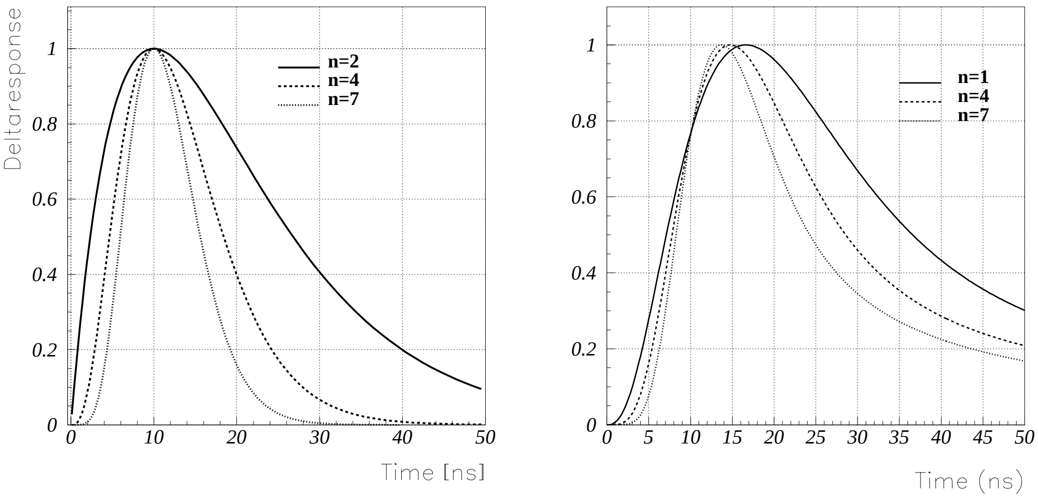

Figure 5.1 *: The left figure shows the front-end delta response for different numbers of integrations. The right figure shows the front-end response to a single ionization electron.*

depend on the front-end chip technology and design. They typically have the values of $e_n \approx 1 - 2\,nV/\sqrt{Hz}$ and $i_n \approx 2 - 3\,pA/\sqrt{Hz}$. If we would be free to chose the delta response $f(t)$ the ENC becomes a minimum for the function

$$f(t)_{opt} = e^{-\frac{|t|}{\tau_c}} \qquad \tau_c = \frac{e_n}{i_n}C \qquad ENC_{min} = \sqrt{e_n i_n C} \tag{5.4}$$

For optimum ENC it is therefore desired to have a delta-response close to this one. For any given detaresponse with a given peaking time t_p the above integral will evaluate to

$$ENC^2 = \frac{1}{2}e_n^2C^2\left(at_p\frac{i_n^2}{e_n^2C^2} + \frac{b}{t_p}\right) \tag{5.5}$$

where a and b depend on the shape of the delta response. The peaking time for minimum noise and the ENC minimum are then given by

$$t_p = \tau_c\sqrt{\frac{b}{a}} \qquad ENC_{min} = \sqrt{e_n i_n C}\,\sqrt[4]{ab} \tag{5.6}$$

so in order to minimize the noise, the delta response shape should be such that the product ab is close to 1, which is the case for symmetric delta responses. For the delta response 5.1 the integral evaluates to

$$a = (\frac{e}{2n})^{2n}(2n-1)! \qquad b = (\frac{e}{2n})^{2n}(n^2(2n-1)! + 2n^3(2n-2)! - n(2n)!) \tag{5.7}$$

the optimum peaking time is given by

$$t_p^{ENC} = \tau_c\sqrt{\frac{b}{a}} = 1,\ 1.15,\ 1.34,\ 1.51,\ 1.67\tau_c \quad \text{for} \quad n = 1,2,3,4,5 \tag{5.8}$$

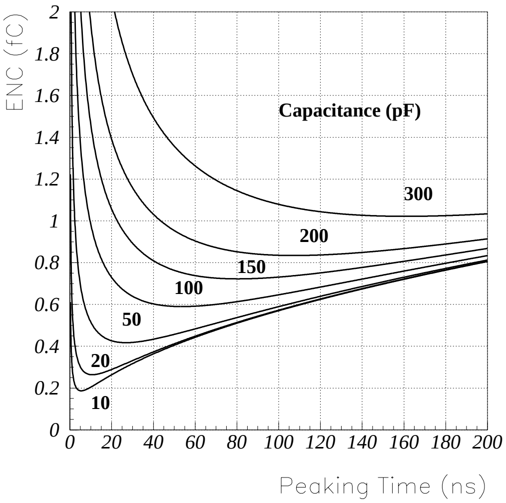

Figure 5.2 *: ENC for different capacitances and n=3 with* e_n=1 $nV/\sqrt{Hz}$ *and* i_n=2.5 $pA/\sqrt{Hz}$.

and the noise at the minimum is given by

$$\sqrt[4]{ab} = 1.35, 1.21, 1.17, 1.16, 1.15 \qquad \text{for} \qquad n = 1, 2, 3, 4, 5 \tag{5.9}$$

We see that for a delta function consisting of 5 integrations the ENC is only 15% higher that the optimum case. Fig. 5.2 shows the dependence of the ENC on t_p for different values of C and n=3.

As stated before the ENC impacts the chamber resolution by imposing a lower limit on the threshold.

5.2 Time Slewing

Different particles traversing the detector will leave different amounts of charge in the chamber. Neglecting diffusion and arrival time spread of the electrons, the signals differ only by their pulse-height, so for the following discussion we assume that ALL the electrons arrive at the SAME time. Due to the finite rise-time of the signal we will measure different times (Fig. 5.3). For a given threshold Thr, a pulse-height P will result in threshold crossing time t according to

$$t = g^{-1}(Thr/P) \tag{5.10}$$

where $g(t)$ is the normalized response of the front-end to a single electron (Fig. 5.1). Therefore a given pulse-height distribution will be mapped into a time distribution. Fig. 5.4 shows the pulse-height distribution from a detailed Monte Carlo study. To estimate the size of the effect we approximate the leading edge of the signal by a straight line (Fig.

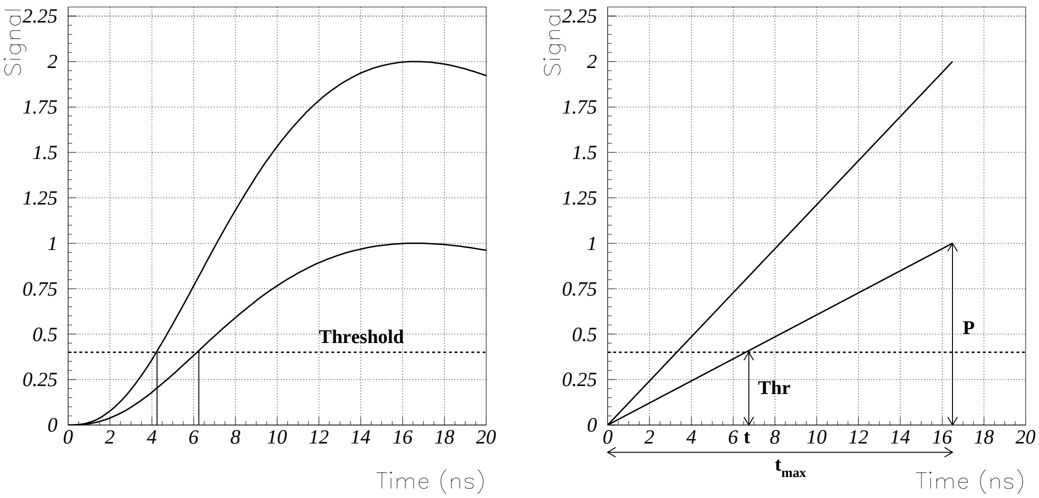

Figure 5.3 *: Pulse-height fluctuations will result in different threshold crossing times (time slewing). Approximating the leading edge by a straight line (right figure) it is evident that the effect will be small for low thresholds and short peaking times.*

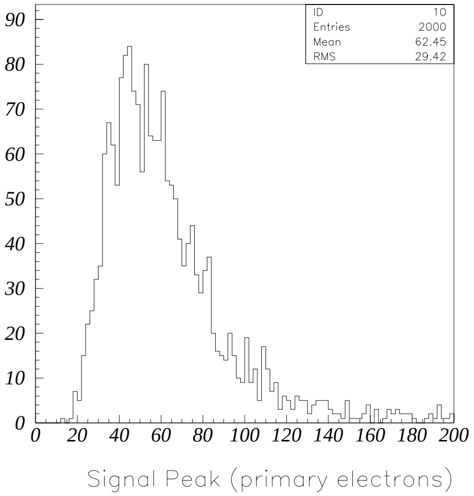

Figure 5.4 *: Pulse-height distribution in a double gap chamber. Since the gap is small the variations are very large.*

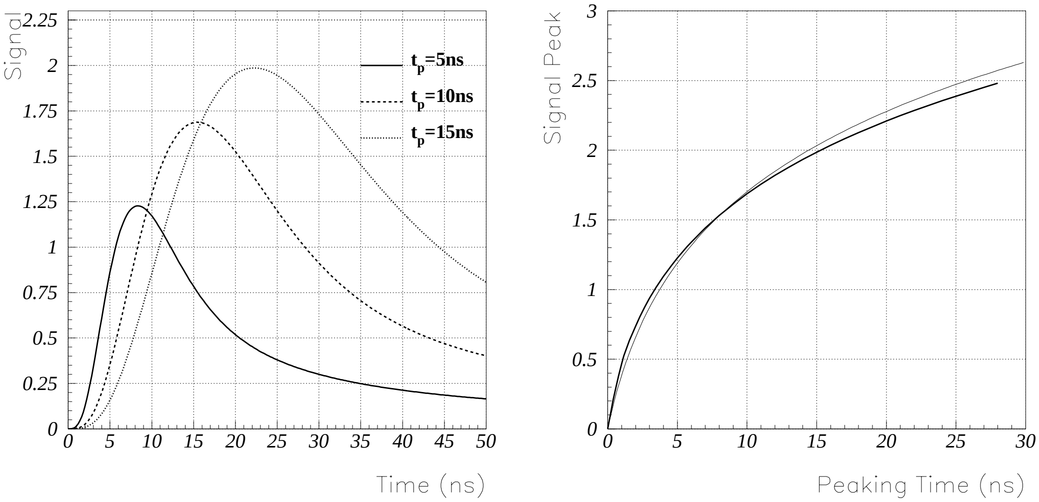

***Figure 5.5** : Response to a chamber signal for different front-end peaking times. The time of the peak is proportional to the peaking time. The dependence of the pulse-height on the peaking time is shown in the right figure.*

5.3). Then the above relation simplifies to (Fig. 5.3)

$$t = Thr/P \times t_{max} \qquad \rightarrow \qquad \sigma_t = \frac{Thr}{P_{av}} \times t_{max} \times \frac{\sigma_p}{P_{av}} \tag{5.11}$$

The time of the signal peak is proportional to t_p, the lowest possible threshold is proportional to the ENC, the average pulse-height is proportional to the gas gain G and the signal peak also depends on tp as shown in Fig. 5.5. The peak is approximately proportional to the charge integrated during the peaking time as given in equation 4.5. Therefore we can write to total time resolution as

$$\sigma_t \propto \frac{t_p e_n C \sqrt{a t_p \frac{i_n^2}{e_n^2 C^2} + \frac{b}{t_p}}}{G \times P_{av} \log(1 + \frac{t_p}{t_0})} \times \frac{\sigma_p}{P_{av}} \tag{5.12}$$

This function has a minimum somewhere between $t_p = 0$ and $t_p = 3.92 t_0$ which represents the optimum front-end peaking time for our system (Fig. 5.6). This result is completely general. If the value $3.92 t_0$ is smaller than t_p^{ENC}, i.e. if for this peaking time the noise is dominated by serial noise which is the case for large capacitances, then the optimum is exactly at $3.92 t_0$ and the above function becomes

$$\sigma_t \propto \frac{e_n C \sqrt{b t_0}}{G \times P_{av}} \times \frac{\sigma_p}{P_{av}} \tag{5.13}$$

For large capacitances the time resolution shows a very weak dependence on the peaking time. This is due to two competing effects: For longer peaking times the noise decreases

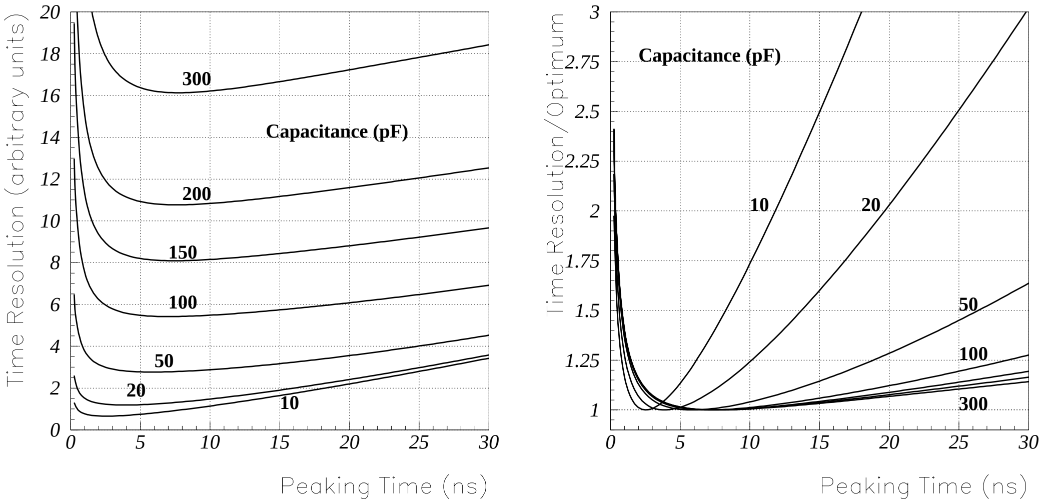

***Figure 5.6** : The right figure shows the timing resolution versus peaking time for different detector capacitances. The left figure shows the same curves normalized to the optimum. We see that the peaking time for best timing resolution is somewhere $< 10\,ns$.*

while the slewing effect increases.

In order to minimize the time slewing we therefore want a small serial noise resistance, small capacitance, high gas gain. The factor b again depends on the shape and is smallest for asymmetric delta responses which is just the opposite of the requirement for a minimum ENC. For the MWPC detector geometry t_0 is 2-3 ns, so the optimum peaking time is around 10 ns.

5.3 Front-end Input Resistance and Capacitance

The capacitance determining the serial noise is the detector capacitance plus input capacitance. Therefore the input capacitance should be as low as possible. The detector capacitance C_{det} together with the front-end input resistance R_{in} define a time constant $\tau_{in} = R_{in}C_{Det}$ which acts as an integration stage. Therefore the chamber signal effectively 'sees' a circuit which consists of an integrator together with the preamp circuit, i.e. R_{in} and C_{Det} decrease the system peaking time. In order to limit this peaking time dependence on the detector capacitance the input resistance should be as small as possible. Low input resistance is also crucial for low crosstalk behaviour which will be discussed in a separate note.

5.4 Tail Cancellation

In the LHCb muon system we expect rates per channel of up to 1.5 MHz. In order to minimize the inefficiency due to signal pile-up the signal pulse-width has to be as short as possible. Since the wire chamber signal has a very long tail we need a dedicated filter circuit to achieve this goal. These filters can be implemented in many different ways. A double pole/zero tail cancellation network is the most popular scheme for wire chamber signals [10].

Chapter 6

Simulation Results

Finally we have all the ingredients to do a full Monte Carlo simulation of the chamber processes. It is important to note that this simulation should mainly give a feeling for the dependence of the performance on the parameters. The final numbers certainly have to be taken from actual measurements. For each event, HEED simulates the charge deposit of the muon in the cell. GARFIELD then drifts the electrons to the wires according to the drift velocity and diffusion as calculated by MAGBOLTZ. The avalanche process is simulated for each electron is simulated and the induced current signal is calculated by tracking the avalanche electrons towards the wire and the ions away from the wire. This signal is then sent through the amplifier by performing a convolution with the amplifier delta-response. The hit-time is finally obtained by applying a threshold to this signal.

The tracks were randomly distributed across the cell. The signals of the wires were combined in OR logic.

Fig. 6.1 shows the preamp response to the four signals from Fig. 4.4. Fig. 6.2 shows the same signals after a double pole/zero network.

From now on we will refer to the threshold in units of ionization electrons i.e. the peak of a single electron signal. Fig. 6.3 shows the time distribution for a peaking time of 10 ns and a threshold of 10 ionization electrons. Fig. 6.5 shows the hit-efficiency and the time resolution for different amplifier peaking times and thresholds. As hit-efficiency we define the fraction of pulses that cross the threshold. Finally Fig. 6.4 shows the average dead-time for different peaking times and integration numbers.

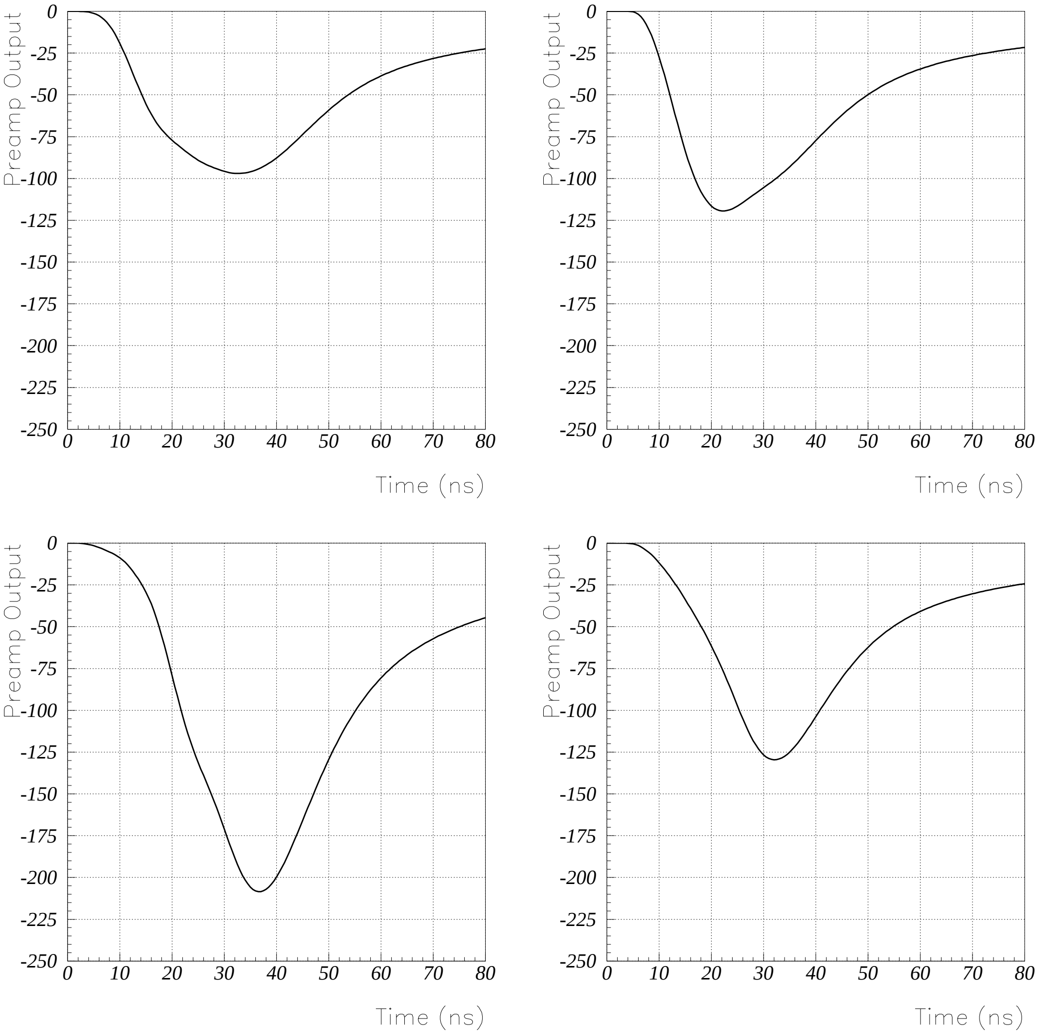

Figure 6.1 *: Preamp output for typical wire signals. The peaking time is 10 ns.*

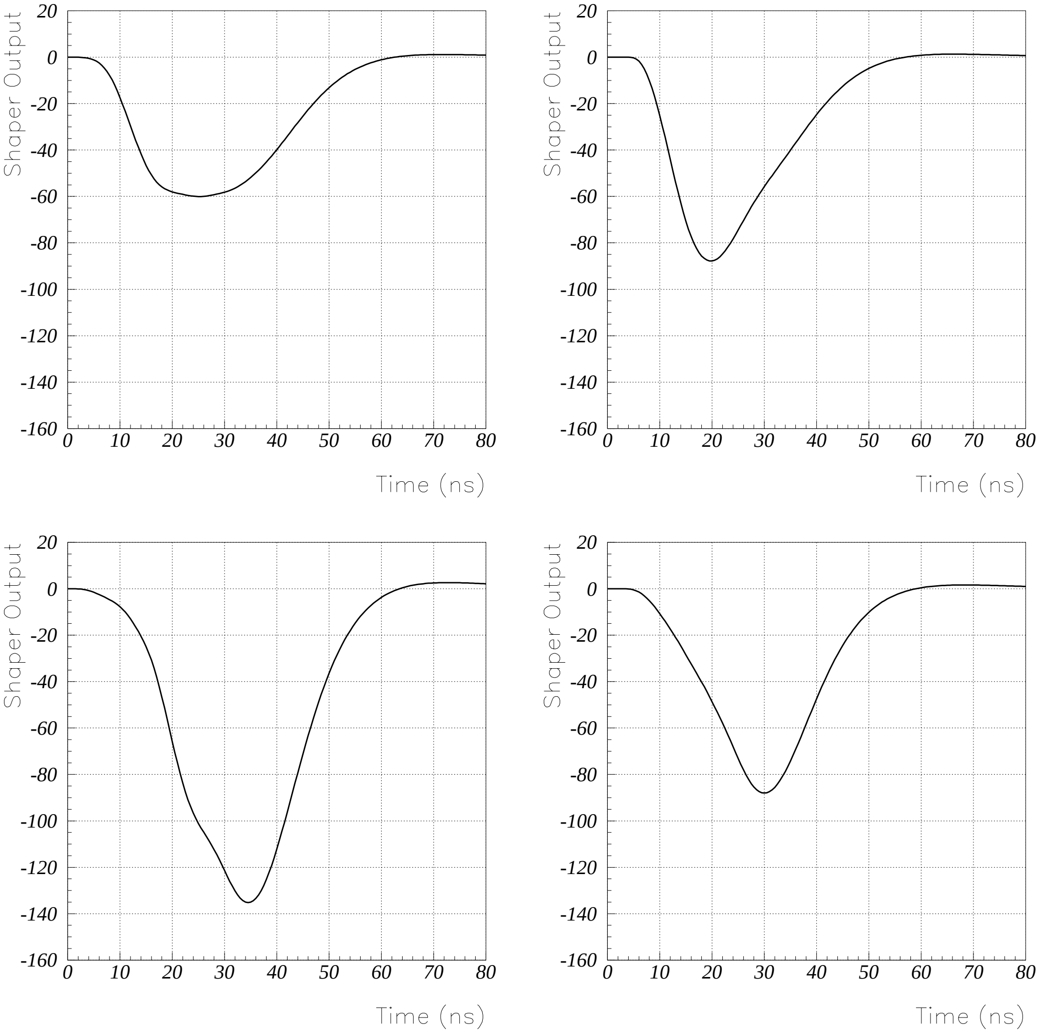

Figure 6.2 *: Shaper outputs for typical wire signals.*

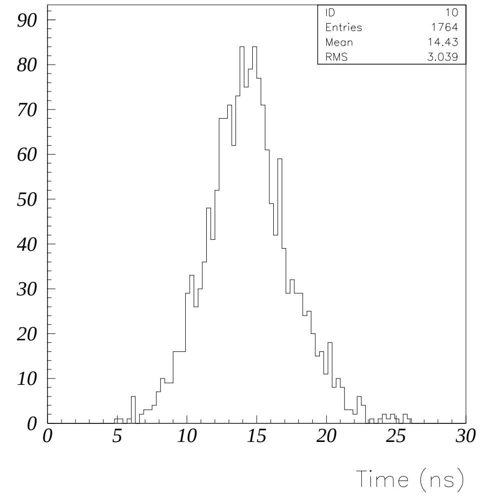

Figure 6.3 : *Time distribution for a peaking time of 10 ns and a threshold of 10 ionization electrons.*

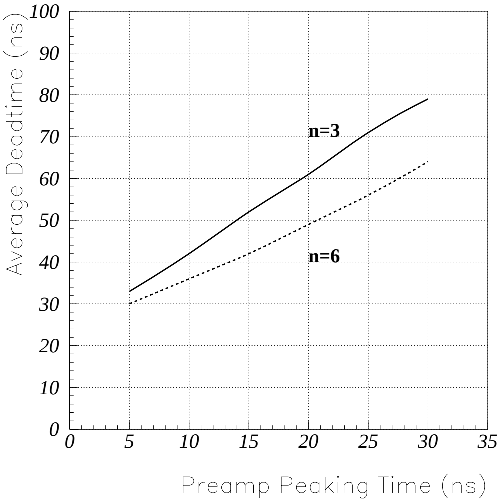

Figure 6.4 : *Average pulse-width for different peaking times and integration numbers.*

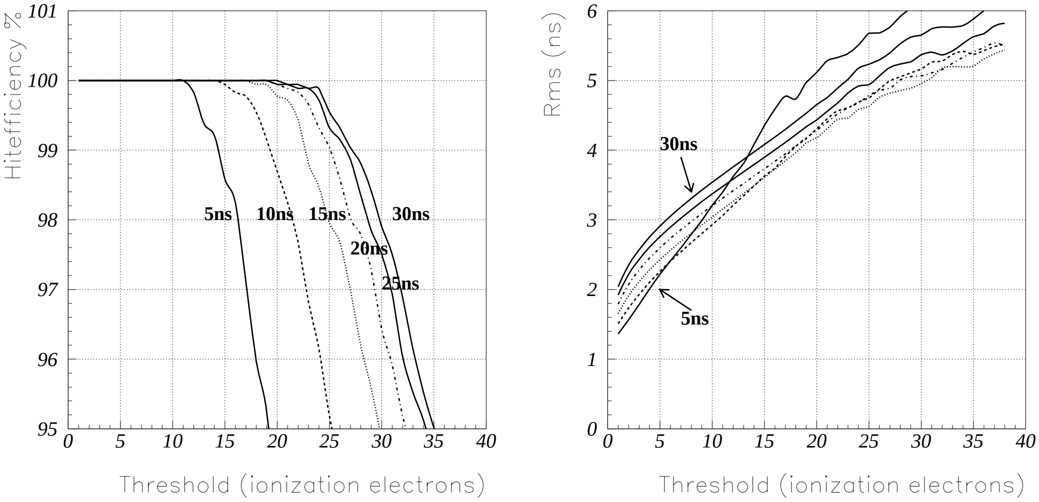

Figure 6.5 *: Hit-efficiency and time resolution for different thresholds and peaking times. The time resolution has a very weak dependence on the amplifier peaking time. The minimum threshold will be given by the noise level.*

Chapter 7

High Rate Effects

7.1 Space Charge Effects

The slow drift velocity of the ions results in a significant build up of space charge in the wire chamber. The main effect is a reduction of the gas gain. The effective voltage drop of a sense wire due to charged particles is given by [2]

$$\delta V = \frac{n_1 q h^2}{2\mu C V_a} \tag{7.1}$$

where C is from (2.4), n_1=count rate per unit length of wire, q = average charge per count, μ=ion mobility. We assume the following parameters: wire diameter $30\,\mu m$, pitch = 1.5 mm, gain 10^5, $\mu = 1.4\,\mathrm{cm}^2/\mathrm{Vs}$, q=$20 \times 2.2 \times 10^5 \times 1.609 \times 10^{-19}\,C$, V_a=3000 V, h=0.25 cm. n_1=$R\times$ pitch where R is the count rate/cm^2.

For these numbers the voltage drop is $1.3 \times 10^{-5} \times R$ Volts. For a rate of 100 kHz/cm^2 we find an effective voltage drop of 1.3 V, so the effect of space charge is negligible.

7.2 Signal Pileup

High counting rates on a channel will result signal pile-up and therefore increased inefficiency. The inefficiency due to pileup for different time resolutions and dead-times is given in Fig. 7.1.

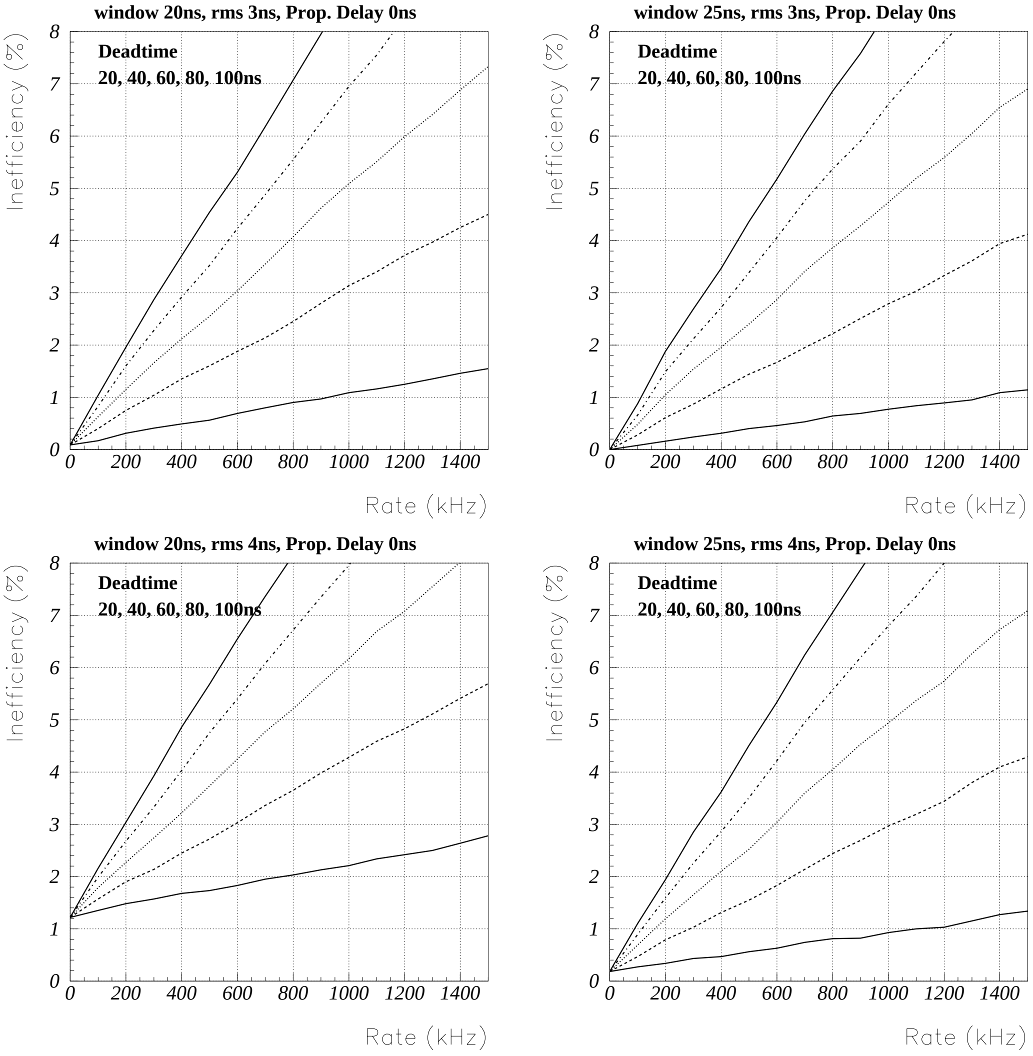

Figure 7.1 *: Inefficiency due to signal pile-up for different rates, time windows and resolutions.*

Chapter 8

Conclusions

- For a chamber with 5 mm gap, 30 μm wire, 1.5 mm pitch at 3.15 kV we have a wire surface field of 260 kV/cm and a cathode surface field of 8.2 kV/cm.
- A 10 GeV muon deposits around 40 clusters with about 2.2 e-/cluster in a double gap chamber, so we find on average around 100 e- in a (5 mm) double gap chamber.
- The gas gain for the above operating point is $\approx 10^5$ and the drift velocity for the gas mixture $Ar/CO_2/CF_4$ 30/60/10 is around 100 $\mu m/ns$.
- A 100 μm guard wire keeps the field on the sense wires constant and has a surface field of 126 kV/cm.
- The cathode charge distribution has a FWHM of ca. 4 mm for a 5 mm gap chamber.
- The arrival time spread of the first electron is around 1 ns for a staggered 5 mm double gap chamber. The average arrival time of the last electron is 25 ns.
- An amplifier peaking time of ca. 10 ns represents an optimum in terms of time resolution and noise.
- The time resolution has a quite weak dependence on the amplifier peaking time.
- The inefficiency due to signal pile-up is around 4 % for a 20 ns gate, pulse-width of 50 ns, 3 ns time-rms and 1 MHz rate.

Thanks to Alexei Vorobyov and Anatoli Kashchuk for very useful discussions.

Bibliography

[1] A. Vorobyov et. al, Wire Pad Chambers for the LHCb muon system, LHCb internal note (2000-003 muon).

[2] E. Mathieson, Induced charge Distributions in proportional detectors, BNL

[3] Rob Veenhof, GARFIELD, a drift chamber simulation program, Version 7.02, CERN

[4] T. Trippe, Minimum tension requirement for Charpak chamber wires, NP Internal Report, CERN 1969.

[5] Anatoli Kachtchouk, private communication

[6] S. Biagi, MAGBOLTZ, program to compute gas transport parameters, Version 2.2, CERN

[7] Igor Smirnov, HEED, program to compute energy loss of fast particles in gases, Version 1.01, CERN

[8] Landolt-Boernstein, vol.4/3, Eigenschaften des Plasmas, no 44315, 6th edn (Springer, Berlin Heidelberg 1957).

[9] Low Noise Techniques in Detectors. V. Radeka, Ann. Rev. Nucl. Part. Sci. 1988, 38, 217, 77

[10] R.A. Boie, A.T Hrisoho and P. Rehak, signal shaping and tail cancellation for gas proportional detectors at high counting rates, NIM 192 (1982).

[11] A. Vorobyov, Wire Pad Chamber Beam test results, talk from June 8 1999

[12] W.Blum, L. Rolandi, Particle Detection with Drift Chambers, Springer Verlag, Berlin-Heidelberg-New York (1993).

[13] S. Ramo, Currents induced in electron motion, PROC. IRE 27, 584 (1939).